Arch. Metall. Mater. **69** (2024), 4, 1585-1591

DOI: https://doi.org/10.24425/amm.2024.151429

G. NARENDER[1], K. CHANDRA SHEKAR[1], YEOLE SHIVRAJ NARAYAN[2],
KODE JAYA PRAKASH[2], B. SRIDHAR BABU[3*]

ORIENTATION INFLUENCE ON TENSILE STRAIN HARDENING IN FORGED PLATES OF AA2014 ALUMINIUM ALLOY

Strain hardening is an effective strengthening method for alloys that requires plastic deformation of the material during manufacturing. The strength will significantly increase due to the number of dislocations formed during plastic flow of material. This study examines the plastic flow activity of forged plates of an AA2014 aluminium alloy with tensile test conditions. The effects of solution treatment and artificial ageing on strain hardening characteristics and tensile behaviour were investigated using tensile testing and scanning electron microscopy. Hollomon plastic flow relationship was employed for solution treated and age hardening conditions by experimental engineering stress- engineering strain data of the aluminium alloy AA2014. In both solution-treated and age-hardened conditions, the alloy displays three distinct strain hardening rate levels.

The highest rate of strain hardening occurs both in solution-treated and age hardening conditions in regions with lower strain. It is also noted that specimens experience higher and lower strain hardening rates in the forging direction (Longitudinal, L) and perpendicular to the forging direction (Transverse, T) respectively in both solution-treated and age hardening conditions. In order to bring out the degree of in-plane anisotropy, test are conducted in L, L+45° (45° to L direction) and T in the plane of forging. Lower and higher magnification SEM images of the alloy under study, clearly exhibited that the ductile dimple fracture associated with a lower shear fracture contributions.

Keywords: Aluminium alloy AA2014; tensile behaviour; ductile fracture; strain hardening; plastic flow; in-plane anisotropy

1. Introduction

Understanding the properties of aluminium alloys in the elasto plastic domain is necessary for their use in structural applications. Plastic strain occurs due to the motion of dislocations, the interaction between these dislocations. The multiplication of dislocations results in increase in the resistance to plastic deformation. The hardening effect can be speeded up due to nano-sized Al_3Sc precipitates distribution [1]. The fracture mechanism and the plastic flow properties of AA2014 aluminium alloy plates under tensile test have been reported [2]. For S30408 austenitic stainless steel, the material's yield strength rises with increasing strain and martensite content following the strain-hardening process. In Al-Mg-Si alloys, two distinctive behaviours usually occur during the elastic-plastic transition.

There is an approximate linear reduction in the work-hardening rate for under heat treated alloys [3]. However, the work-hardening rate remains constant followed by an total linear decrease for over heat treated AA 6061 Al alloys after elastic-plastic transformation [4-5]. This work investigates the strain-hardening characteristics of forged aluminium alloy AA2014 under solution-treated and peak-heat treated (aged) conditions. The Hollomon model is fitted with uniaxial tensile test results. The study concludes by presenting the influence of aging on the plastic deformation and strain-hardening behaviour of AA2014 aluminium alloy. The tensile fracture surface reveals ductile fracture with remarkable changes in shape and size of dimples.

2. Experimental

2.1. Material

The material under investigation in this work is the aluminium alloy AA2014, recognized as an Al-Cu-Mg-Si alloy.The

[1] DEPARTMENT OF MECHANICAL ENGINEERING, VIGNAN INSTITUTE OF TECHNOLOGY AND SCIENCE, HYDERABAD-508284, INDIA
[2] DEPARTMENT OF MECHANICAL ENGINEERING, VNR VIGNANA JYOTHI INSTITUTE OF ENGINEERING AND TECHNOLOGY, HYDERABAD, INDIA
[3] DEPARTMENT OF MECHANICAL ENGINEERING, MALLA REDDY ENGINEERING COLLEGE, HYDERABAD, INDIA

* Corresponding author: bsridhar7777@gmail.com

composition of the alloy forging is 4.4% Cu, 0.8% Mn, 0.8% Si, 0.4% Mg and 93.6% Al. The composition was found to be within the specified limit range of the aluminum alloy AA2014 standard composition. The important significant alloying element for aluminum is copper because of its solubility and reinforcing effect. Higher strengths have been obtained in binary aluminium copper alloys due to relatively more silicon percentage, thus increasing the ability to strain hardening during artificial ageing. The alloy under investigation is especially suitable for high strength to weight ratio parts and structures and has wide applications in structural components of aero industries, automobile wheels and parts that should have sufficient strength up to 150°C. The alloy exhibits limited weldability with good machinability.

2.2. Tensile testing

Using an EDM wire cutting machine, the required number of specimens measuring 170 mm × 105 mm × 4 mm were cut and then solutionized and heat treated. Desired orientation of tensile specimens was made from the forged block shown in Figure 1.Strengthening results from the precipitation-hardening process, which is achieved by solutionizing at an appropriate temperature and then quenching. Hence these specimens were solutionized at 502±5°C for 55 minutes and quenched in 64°C hot water to prevent disfigurement. After solutionization separately, some plates were heat treated for 10 h at 177±3°C in the furnace, which were designated as peak heat treated (aged) specimens. **Infrared heat treatment was used as a rapid heating technique to effectively replace the conventional resistance heat treatment method. Infrared heat treatment resulted in better age hardening at the initial aging stage, where its tensile strength and elongation appeared like that of a resistance heat treatment** [6].

The specimens for tensile testing were cut in three directions from the solutionised and heat treated plates *L* (in the direction of forging), L+ 45° (45° to the direction of forging), and *T* (perpendicular to the direction of forging), as shown in Fig. 1. Tensile tests were conducted using the INSTRON 5500R-4507-250 kN universal testing system at a cross-head speed of 1 mm/minute. The specimens utilized for the tests were E-8 specimens, as per the ASTM Standard E-8, 2013, and are illustrated in Fig. 2. In each sample direction, two specimens were tested and the mean values of 0.2% yield strength (σ_Y), ultimate tensile strength (σ_{UTS}) and percentage elongation were determined.

3. Results

3.1. Tensile properties

Fig. 3 displays the engineering stress-engineering strain diagram in solution-treated condition, age hardening condition-sup to the breaking point of the alloy specimens under analysis.

There are variations in the values of ultimate tensile strength (σ_{UTS}), yield strength (σ_Y), total elongation percentage and strain hardening exponent (n) in three test directions. The strain hardening exponent 'n' is determined using Hollomon equation,

$$\text{Flow stress, } \sigma = K\varepsilon_p^n$$

The σ_Y and σ_{UTS} values are observed to be maximum in the perpendicular to forging direction (L + 90°) and minimal in the L + 45° direction in the solution-treated condition as well as peak heat treated (TABLES 1 and 2).

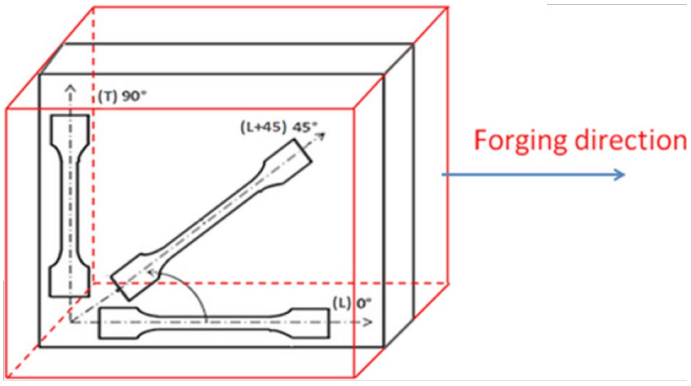

Fig. 1 Schematic figure showing the specimen code adopted forthe evaluation of in-plane anisotropy in tensile deformation

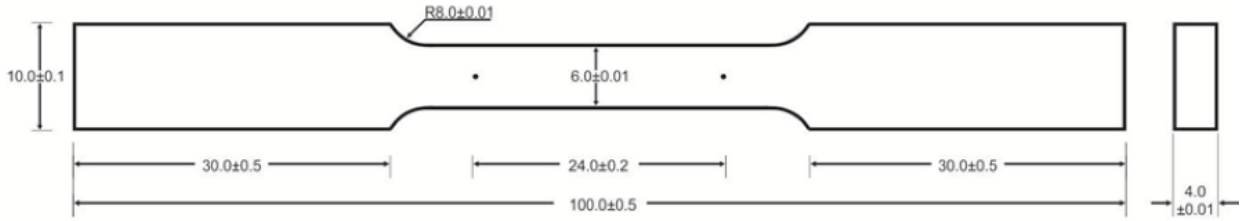

Fig. 2 Specimen for tensile testing (all dimensions are in mm)

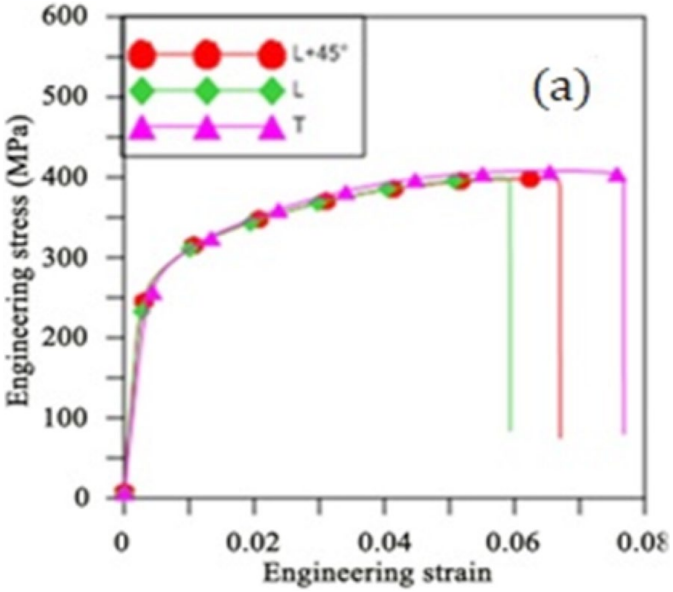

Fig. 3(a). Engineering stress-engineering strain diagram of solution treated condition

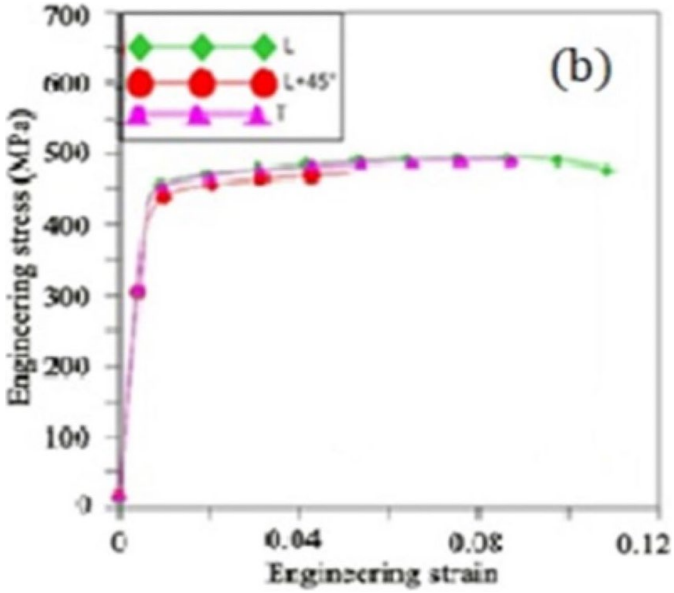

Fig. 3(b). Engineering stress-engineering strain diagram of peak aged condition

TABLE 1

Tensile properties of aluminium alloy AA2014 plate in solution treated condition

S. No.	Property	Specimen orientation with respect to the forging direction, Deg.		
		L	*L* + 45°	*T*
1	0.2 % Y.S, MPa	277.1	276.3	281.8
2	UTS, MPa	399.6	398.7	408.7
3	Total Elongation, % (24 mm gauge length)	19.6	20.7	18.4
4	Strain Hardening exponent *n*	0.13614	0.13704	0.18217
5	Value of σ_{UTS} / σ_Y	1.442	1.443	1.450

TABLE 2

Tensile properties of in solution treated and peak agedcondition

S. No.	Property	Specimen orientation with respect to the forging direction, Deg.		
		L	*L* + 45°	*T*
1	0.2 % Y.S, MPa	450.1	422	447.2
2	UTS, MPa	496.4	472.8	492.3
3	Total Elongation, % (24 mm gauge length)	11.04	5.32	8.92
4	Strain Hardening exponent *n*	0.05678	0.04751	0.05013
5	Value of σ_{UTS} / σ_Y	1.1026	1.1181	1.1169

3.2. Fracture mode

To evaluate the mode of fracture of tensile test specimen, scanning electron microscope is used. Figs. 4 and 5 display the broken surfaces of solution treated and peak heat treated specimens, respectively. In combination with elongated grains, the SEM images in Fig. 4 display the fibrous fractured surface.

The range of values for the strain hardening exponent is 0 to 1. A substance with a value of 0 is completely plastic, whereas a material with a value of 1 is 100% elastic. An alloy's "*n*" value is typically between 0.10 and 0.15.

3.3. Strain hardening evaluation

True stress (flow stress) (σ) and true plastic strain (ε) data from tensile tests are used to characterize the behavior of strain hardening. The variations of strain hardening parameters and tensile true plastic strain exhibited three distinct regimes. The instantaneous strain hardening rate $\theta = (d\sigma/d\varepsilon)$ can be determined by tensile true stress (σ) – true plastic strain (ε) at each experimentally determined point. The strain hardening exponent '*n*' is a material constant and obtained from the **Hollomon** equation.

4. Discussion

4.1. Tensile behaviour

The yield strength and elongation are the most critical in-plane anisotropic tensile properties in crystallographically symmetric face centered cubic metals like aluminium, aluminium-lithium (Al-Li), and Nimonic alloys. The presence of a robust crystallographic texture and grain fibers contributes to in-plane anisotropy [7-8]. In the case of Nimonic C-263 alloy, in a state of being cold-rolled and solution-treated, the highest and lowest yield strength values are observed along the rolling direction (*L*) and perpendicular to the rolling direction (*T*), respectively. Conversely, Al-Li alloys exhibit a lower yield strength value in the 45°-60° direction compared to the *L* and *T* directions [9].

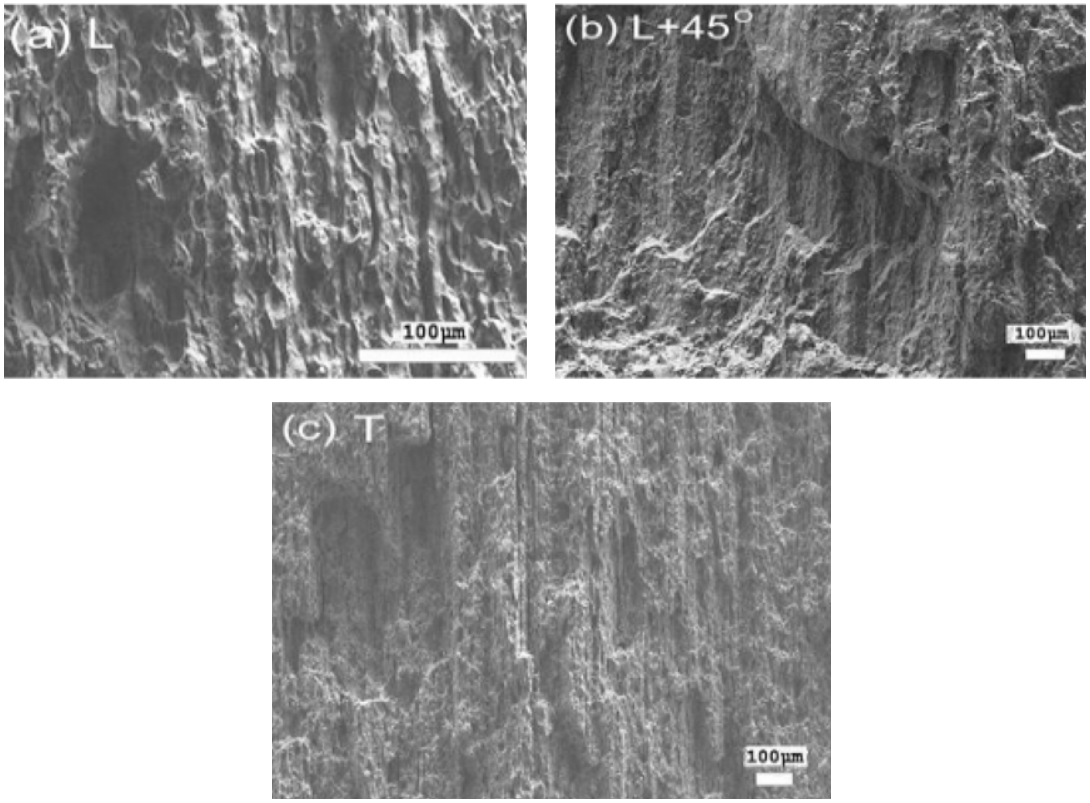

Fig. 4. Low magnification SEM image of fractured tensile tested specimens in solution treated condition in three test orientations

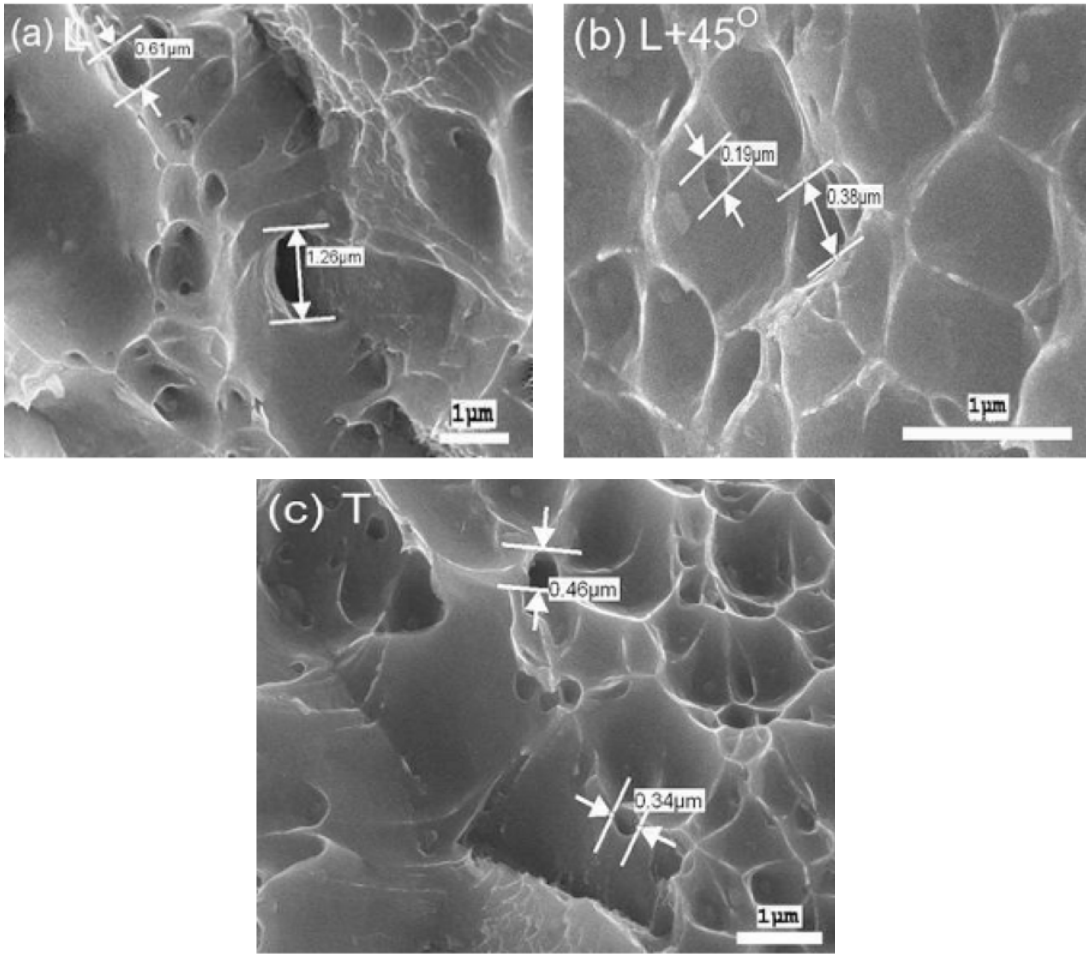

Fig. 5. High magnification SEM image of fractured tensile tested specimens in solution treated peak aged condition in three test directions

For the Ni-based Hastelloy C-276 alloy, it was noted that the highest and lowest values of yield strength (σ_Y) were observed along the rolling direction (L) and at a 45° angle to the rolling direction (L + 45°) [10]. The stress-strain behaviours of AA 5083-H112/6061-T6 materials through conducting tensile tests on 32 AA coupons at 20℃ ~ −165℃. All the tested AA coupons exhibited ductile failure modes. Their results showed that the stress-strain curves of AA 5083-H112 exhibited the Portevin-Le Chatelier effects that gradually weakened with the decreasing temperature. Reducing the temperature from 20℃ to −165℃ increased the elastic modulus, yield and ultimate strengths of AA 5083-H112 (or 6061-T6) by 5.1% (6.5%), 8.7% (12.0%) and 7.8% (13.1%), but reduced the fracture strain by 16.4% (12.4%) [11-13]. Aging does not alter the behavior of macroscopic flow, it does result in significant changes in all parameters related to plastic deformation as well as microstructural changes. Fig. 3 shows the variance of percentage elongation, σ_{UTS} and σ_Y with the angle of forging direction, clearly showing the anisotropy of the material being studied. The initial linear region of the stress-strain curve corresponds to the elastic deformation of the material, where the deformation is recoverable upon the removal of the applied load. As the applied load increases, the material enters the plastic deformation region, where the stress increases nonlinearly with strain. This is due to the dislocation motion and multiplication within the material, which leads to the formation of strain hardening. The shape and trend of the stress-strain curve for aluminium alloys can be further influenced by various factors such as strain rate, temperature, and microstructural features like grain size and texture. During initial deformation, cross slip of planes takes place along with formation of cells.

4.2. Fracture behaviour

It has been observed that in solution-treated specimens, the failure takes place at the grain boundaries. Fig. 4 shows clearly that under tensile test loading, the alloy plates fail through high-intensity ductile void fracture associated with fracture in shear plane.Initially, the density of dimples decreases as the position varies from 0-45° and then increases afresh. Also, very thin micro dimples, which are spread equally, are visible in SEM images. The spread of fine and coarse dimples of different sizes and shapes contributing to total micro void coalescence. This due to the formation of void-nucleation and development of coalescence. With typical ductile characteristics in given three test orientations, the tensile fracture surfaces show major variations in the shape and size of the dimples from the direction of forging (L) to its perpendicular direction (T) (Fig. 5). The dimples have a spherical shape when along L; however, they take on as elongated appearance when the test orientation is shifted to L + 45° and then to T direction. (Fig. 5). The scale of the dimples decreases too slowly from the direction of forging (L) to its perpendicular direction (T).

Fracture, on a microscopic scale, was predominantly ductile comprising micro void nucleation, growth and coalescence. As the tensile stress increases, plastic deformation becomes more localized within the necked region. This localized deformation is accompanied by significant strain localization and the development of shear bands or localized necking. Within the highly strained regions, such as shear bands or near grain boundaries, microvoids start to form due to the accumulation of plastic strain. As deformation continues, these microvoids grow in size and coalesce with neighbouring voids, leading to the formation of larger voids or cavities. This process of void growth and coalescence further concentrates stress within the material, leading to the propagation of cracks [14].The formation of micro-voids and their nucleation during tensile deformation provide an explanation for this phenomenon.

Strong continuous elongation in the forging direction is associated with small-scale nucleation and strong micro-void formation (L). Consequently, for peak heat treated status, there is maximum elongation along the direction of forging (L). In addition to ductile characteristic and the strain-hardening exponent, there is an increase in the fraction of micro void.

4.3. Strain hardening behavior

It was reported that Nickel-based super alloy SUPERCAST 247A there are two separate stages of strain hardening under various heat treatment processes [15]. Figs. 6a and 6b show the the relation between rate of strain hardening, $\theta = (d\sigma/d\varepsilon)$ and true plastic strain of solution treated and aged conditions. This data indicate that, under both solution-treated and heat-treated conditions, the strain hardening behavior of the alloy can be delineated into three distinct segments. In segment I, the strain hardening rate initially decreases, followed by a constant rate in segment II, and a subsequent decrease in segment III. Interestingly, the strain hardening rate curves converge for the solution-treated and heat-treated conditions at higher true plastic strain values and in regions of elevated true stress.

Figs. 6a and 6b show that specimens in the direction of forging (L) exhibit higher levels of strain hardening rate i.e. 17950 MPa, while T directional specimens exhibit lower rate of strain hardening i.e. 16350 MPa in solution-treated condition. Similarly in case of peak aged specimen in the direction of forging (L) exhibit higher levels of strain hardening rate i.e. 19750 MPa, while T directional specimens exhibit lower rate of strain hardening i.e. 10500 MPa. It can be interpreted that there is difference in the rate of work hardening in the three segments of the alloy under study because of the sub-structural properties in the low stalking fault energy alloys [16-17]. Dynamic recovery in segment I cause the reduction in the rate of strain hardening due to cross-slip and extinction of screw dislocation constituents. Initial twinning deformation in the microstructure begins, which causes segment II strain hardening rate to remain constant. The deformation twin boundaries start to form at the beginning of segment II. These help to form regions for dislocation pile up and storage at grain boundaries. For every system that intersects the twins, slip dislocations multiply and

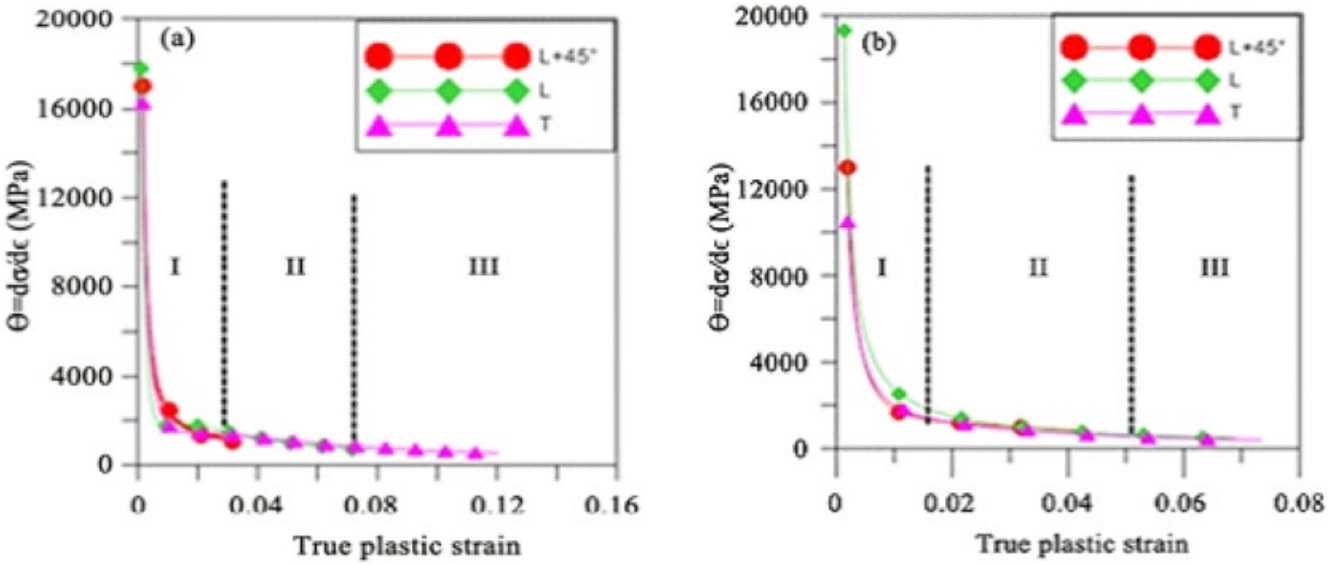

Fig. 6. (a) Strain hardening rate $\theta = (d\sigma/d\varepsilon)$ vs. true plastic strain in solution treated condition and (b) Strain hardening rate $\theta = (d\sigma/d\varepsilon)$ vs. true plastic strain in peak aged condition in various specimen orientations. The strain hardening rate, denoted as plotted against true plastic strain in the solution-treated condition

spread. The slip distance formed is very less compared to the original grain size. A factor in decrease in grain size is due to the formation of twins. In segment II, the overall strain hardening rate remains almost constant, resulting from a uniform rise in density of formation of twins, with strain steadily reducing gaps between slip. Previous studies indicated that in segment III there is a reduction in rate of basic twin formation that contributes to a decrease in the strain hardening rate [18]. It is found that the alloys Ti-6Al-4V and CP-Ti exhibit moderate strain hardening behavior. At a certain temperature, the strain hardening **index**(n) increases with increasing strain rate; but, for a given strain rate, it decreases with increasing temperature [19].

Dislocation slip and deformation twinning can be combined and further controlled, for ongoing work strengthening [20]. The tensile strength, tensile ductility and work hardening characteristics of AISI 431 martensitic stainless steel varied in separate intermediate and high temperature regimes [21]. A technique known as continuous bending under tension, or CBT-FEM, was developed to understand how an aluminium alloy, specifically AA6022-T4 sheets, would behave while strain hardening after necking. A proposed simplified multi-stage constitutive relation that combines the Hollomon and Ramberg-Osgood models is presented to explain the non-linear strain hardening behavior observed in the full-range stress-strain curve. There is difficulty propagating recent basic twins with strain in segment III. In this case, it reduces the distance a twin will develop before contacting an obstacle. This leads to a decrease in the size of the grain, which leads to more difficult in twining. It is evident that higher stresses are needed for nucleating with smaller grains. The drop in the rate of strain hardening beyond some limit in segment III (~4 percent) is due to rise in twin density with strain leading to a gradual decrease in the inter twin gap. This also makes it difficult to nucleate twinning there by contributing to a decrease in the rate of strain hardening in segment III.

5. Conclusions

1. The data obtained from tensile test of AA2014 aluminium alloy in solution- treated and age hardening conditions were analysed using the Hollomon equation and strain hardening **index** were calculated.
2. The maximum strain hardening rate is found along the forging direction (L) and the minimum is found perpendicular to the forging direction (T) in solution-treated and age-hardened alloy specimens.
3. The tensile fracture surfaces of all three in-plane test directions, displaying classic ductile characteristics. There is a lot of variation in shape and size of the dimples in three test directions in both solution- treated and age hardening conditions. All these dimples formed due to micro-void nucleation, growth of voids and coalescence, leading to gross dimple fracture.

Acknowledgements

The authors express gratitude to the Sophisticated Analytical Instruments Facility (SAIF) at IIT Bombay for their valuable support in conducting SEM studies. Additionally, appreciation is extended to the RegionalCentre for Military Airworthiness (RCMA), DRDO, Hyderabad, for generously providing facilities for heat treatment, optical microscopy, and hardness testing. Special thanks are also due to the Advanced Materials Testing Laboratory (AMTL), Hyderabad, for their assistance in conducting tensile testing.

REFERENCES

[1] P.K. Mandal, Study on hardening mechanisms in aluminium alloys. Int. J Eng. Res. Appl. **6** (1), 91-97 (2016).

[2] G. Narender, E. Ramjee, N.E. Prasad, In-plane anisotropy and tensile deformation behaviour of aluminium alloy AA2014 forge plates. Sadhana **44** (22), 125-135 (2019).
DOI: https://doi.org/10.1007/s12046-018-0994-8

[3] Bo Li et al., The effect of strain hardening on mechanical properties of s30408 austenitic stainless steel: a fundamental research for the quality evaluation of strain strengthened pressure vessel. IOP Conf. Ser.: Mater. Sci. Eng. **382**, 032013 (2018).
DOI: http://doi.org/10.1088/1757-899X/382/3/032013

[4] A. Bahrami, A. Miroux, J. Sietsma, Modeling of strain hardening in the aluminum alloy AA6061. Metall. Mater. Trans. A. **44**, 2409-2417 (2013).
DOI: https://doi.org/10.1007/s11661-012-1594-6

[5] ASTM Standard E-8, Standard test methods for tension testing of metallic materials, ASTM International, West Conshohocken, PA, 2013.

[6] Y.L. Chang, F.-Y. Hung, T. Lui, A New Infrared Heat Treatment on Hot Forging 7075 Aluminium Alloy: Microstructure and Mechanical Properties. Materials **13**, 1177-1185 (2020).

[7] K. Ankamma, A.K. Singh, K.S. Prasad, G. Chandramohan Reddy, M. Komaraiah, N.E. Prasad, Effects of aging and sheet thickness on the room temperature deformation behaviour and in-plane anisotropy of cold rolled and solution treated Nimonic C-263 alloy sheet. Int. J. Mat. Res. **102**, 1274-1285 (2011).
DOI: https://doi.org/10.3139/146.110573

[8] N.E. Prasad, G. Malakondaiah, Anisotropy of mechanical properties in quaternary Al-Li-Cu-Mg alloys. Bull. Mater. Sci. **15**, 297-310 (1992).

[9] N.E. Prasad, In-plane anisotropy in the fatigue and fracture properties of quaternary Al-Li-Cu-Mg Alloys. Dissertation, Banaras Hindu University Varanasi, India (1993).

[10] K.V. Jata, S. Panchandeeswaran, A.K. Vasudevan, Evolution of texture, microstructure and mechanical property anisotropy in an Al-Li-Cu alloy. Mat. Sci. Eng. A. **257**, 37-46 (1998).

[11] K.K. Mehta, M. Prantik, R.K. Mandal, A.K. Singh, Mechanical properties anisotropy of cold rolled solution-annealed Ni-based Hastalloy C-276. Met. Mat. Trans. **45**, 3493-3514 (2014).
DOI: https://doi.org/10.1007/s11661-014-2294-1

[12] Rong Xi, Jian Xie, Jia-Bao Yan, Evaluations of low-temperature mechanical properties and full-range constitutive models of AA 5083-H112/6061-T6. Construction and Building Materials, 411-413 (2014).

[13] T S Srivatsan, S Sriram, D Veeraraghavan et al. Microstructure, tensile deformation and fracture behaviour of aluminium alloy 7055. Journal of Materials Science **32**, 2883-2894 (1997).

[14] A. Lavakumar, CHVS Murthy, D.V.V. Satyanarayana, N.E. Prasad, Strain hardening behaviour of a nickel based superalloysupercast 247A. Int. J. Sci. Engg. Res. **4**, 1914-1920 (2013).

[15] D.C. Ludwigson, Modified stress-strain relations for FCC metals and alloys. Met. Tran. **2**, 2825-2828 (1971).

[16] D.V.V. Satyanarayana, K. Satya Prasad, G. Malakondaiah, D.S. Sarma, Strain hardening behaviour of an Fe–Ni–Cr–Al alloy. Mat. Sci. Tech. **23**, 79-86 (2007).

[17] R.K. Gupta, Mathew Chirsty, P. Ramkumar, Strain hardening in aerospace alloys. Front Aerospace Eng. **4**, 1-12 (2015).

[18] A. Grajcar, A. Kozłowska, B. Grzegorczyk, Strain hardening behavior and microstructure evolution of high-manganese steel subjected to interrupted tensile tests. Metals **8** (2), 122-128 (2018).
DOI: https://doi.org/10.3390/met8020122

[19] E.I. Samuel, P. Neeta, M. Nandagopal, S.P. Selvi, S.N. Narendra Babu, S.L. Mannan, Tensile deformation and work hardening behaviour of AISI 431 martensitic stainless steel at elevated temperatures. High Temp. Mater. Proc. **38**, 916-926 (2019).

[20] C. Poulin, T. Barrett, M. Knezevic, Inferring post-necking strain hardening behavior of sheets by a combination of continuous bending under tension testing and finite element modeling. Exp. Mech. **60**, 4, 59-473 (2020).

[21] S. Digendranath, S.K. Selvan, B.P. Thomas, A.K. Asraff, J. Philip, Full-range stress-strain model for metallic materials depicting non-linear strain-hardening behaviour. J. Strain Anal. Eng. Design **10** (2020).
DOI: https://doi.org/10.1177/0309324720957798